JOURNAL OF COMPUTATIONAL PHYSICS 52, 480–502 (1983)

Implicit Particle Simulation of Magnetized Plasmas

D. C. BARNES, T. KAMIMURA,* J.-N. LEBOEUF, AND T. TAJIMA

Institute for Fusion Studies, University of Texas, Austin, Texas 78712

Received October 6, 1982; revised May 3, 1983

An accurate, direct method for the simulation of magnetized, multi-dimensional plasmas is developed. A time decentered particle push is combined with the direct method for implicit plasma simulation to include finite sized particle effects in an absolutely stable (under conditions for which the field corrector converges) algorithm. Second-order temporal accuracy is attained when the decentering parameter may be chosen smaller than the normalized frequency of interest. A simple iteration (renormalized Poisson equation) is used to solve the field corrector equation. Details of the two-dimensional, electrostatic, constant magnetic field, periodic case are given. Numerical results for ion-acoustic fluctuations and for an unstable gravitational interchange confirm the accuracy and efficacy of the method applied to low-frequency plasma phenomena.

I. INTRODUCTION

Current plasma confinement experiments provide many examples of low-frequency phenomena in which kinetic effects are all important. Drift frequency fluctuations in a low-β plasma are correctly described only by considering the effects of finite ion gyroradius and resonant electron motion. A similar situation occurs in considering collisionless tearing modes at either macroscopic or microscopic scales. For slightly higher frequency modes, the interaction of kinetic effects with MHD instabilities must be considered to study stability of the Bumpy Torus or Tandem or Field Reversed Mirror plasma. These modifications to MHD behavior may also be important in Tokamak confinement where kinetic effects on ballooning modes may allow higher β operation.

In this paper a recently developed algorithm for multi-dimensional plasma simulation of such low-frequency phenomena is described. These phenomena are those whose characteristic frequency (mode frequency) ω is smaller than either the plasma frequency ω_α or cyclotron frequency Ω_α for one or several species α ($\omega \ll \omega_\alpha, \Omega_\alpha$).

The algorithm described differs from conventional particle simulation methods [1], which accurately and efficiently represent short time scale plasma phenomena, in that time steps Δt much larger than ω_α^{-1} or Ω_α^{-1} are employed. In this way a practical

* Permanent address: Institute of Plasma Physics, Nagoya University, Nagoya, 464 Japan.

0021-9991/83 $3.00

number of time steps can represent the long time scales of interest ($\omega_\alpha \Delta t$, $\Omega_\alpha \Delta t \gg 1$, $\omega \Delta t \lesssim 1$).

In contrast to single or multiple fluid plasma simulations [2], which effectively represent phenomena of confined plasmas on very long time scales by moment equations, the algorithm described here retains all low-frequency kinetic effects by accurately following single particle orbits.

The possibility of using implicit field computations, in which the particles are accelerated in an electromagnetic field determined by time advanced particle data, was considered by Langdon [3]. There it was concluded that a direct inversion of the implicit particle difference equation was impractical. Mason [4] showed that including the time-advanced plasma response only through the cold fluid response was sufficient for stability. This ingenious algorithm avoided the full matrix inversion and demonstrated the practicality of one-dimensional electrostatic plasma simulation for $\omega_e \Delta t \gg 1$. Alternative formulations of implicit plasma simulation algorithms have been described and analyzed for the one-dimensional electrostatic case [5–8]. Brackbill and Forslund [9] have extended these methods to the two-dimensional electromagnetic case, using the moment equation method [4].

The distinguishing features of the algorithm described here are as follows. First, the difference equations of motion are second-order accurate for small $\omega \Delta t$, and the numerical damping of such low-frequency modes is much smaller than that for first-order accurate methods. Second, the implicit equations are formulated using the direct method [6–8] with simplified differencing. This allows the consistent inclusion of finite size particles so that long wavelength modes are very accurately represented with relatively few particles per cell. Third, a simple method [10] for simulation of strongly magnetized plasmas ($\Omega_e \Delta t \gg 1$) is combined with the implicit electrostatic field method. Finally, a very simple technique for iteratively solving the implicit field corrector equation based on the renormalized particle code method [11] is implemented for the two-dimensional magnetized plasma.

Although the method described here may be applied to fully electromagnetic plasma simulation [12] and may include finite gyroradius effects for arbitrarily large time steps [10, 13], the present paper is limited to a description of the simplest multi-dimensional algorithm. For this purpose, the electrostatic approximation is made, the static magnetic field is taken to be uniform, and all effects of finite gyroradius are neglected. In addition, the spatial boundaries are taken as periodic throughout.

The plan of the remainder of the paper is as follows. In Section II the implicit plasma method is developed, and several issues associated with accuracy, numerical damping, and implementation of this algorithm are addressed. In Section III numerical results for ion-acoustic fluctuations in a thermal plasma and for a gravitationally driven interchange mode are presented and the accuracy of these results discussed. Finally, in Section IV conclusions are drawn and future directions for extension are outlined.

II. Numerical Method

a. *Normalized Difference Equations*

Following the finite size particle method [1, 3], a collisionless plasma is represented by the motion of a large number of superparticles, which move in accordance with the equations of motion (rationalized MKS units are employed here)

$$\dot{\mathbf{x}}_j = \mathbf{v}_j, \tag{1a}$$

$$\dot{\mathbf{v}}_j = \mathbf{A}_\alpha(\mathbf{x}_j, t) + \mathbf{v}_j \times \boldsymbol{\Omega} \tag{1b}$$

for $j = 1,..., N_0$, and the species index $\alpha = e, i$. In Eq. (1) the super dot indicates the usual time derivative and $\mathbf{A}_\alpha$ is the electric acceleration felt by the particle of species α

$$\mathbf{A}_\alpha(\mathbf{x}, t) = (q/m)_\alpha \int d\mathbf{x}'\, h(\mathbf{x} - \mathbf{x}')\, \mathbf{E}(\mathbf{x}', t), \tag{2}$$

where h is the particle shape. Also in Eq. (1), $\boldsymbol{\Omega}_\alpha = (q/m)_\alpha \mathbf{B}$ is the cyclotron frequency (vector). Although $\boldsymbol{\Omega}_\alpha$ may depend on $\mathbf{x}$ and t in the general case, $\boldsymbol{\Omega}_\alpha$ is taken as a static constant in the present paper.

The self-consistent plasma model is completed by the appropriate Maxwell equations. For the electrostatic approximation taken here, these are

$$\mathbf{E} = -\nabla\phi, \tag{3a}$$

$$\nabla^2\phi = -\rho, \tag{3b}$$

$$\rho = \sum_j q_j h(\mathbf{x} - \mathbf{x}_j). \tag{3c}$$

To solve the field Eq. (3), a grid is introduced in the usual way and particle quantities are interpolated to and from this grid. Thus, for a set of grid points $\mathbf{x}_g$ the difference operators in Eq. (3) are evaluated by finite differences or finite Fourier transforms (details are given below). The particle shape h is interpolated as $h(\mathbf{x}_g - \mathbf{x}_j) \sim \sum_{g'} h(\mathbf{x}_g - \mathbf{x}_{g'})\, i(\mathbf{x}_{g'} - \mathbf{x}_j)$, for some interpolation function i. This determines the "raw" charge density

$$n_\alpha = \sum_{j\,\alpha} q_j i(\mathbf{x}_g - \mathbf{x}_j), \tag{4}$$

the sum taken over all particles of species α. In terms of n_α, ρ is given by a convolution with h,

$$\rho_\alpha = H^* n_\alpha \equiv \sum_{g'} h(\mathbf{x}_g - \mathbf{x}_{g'})\, n_\alpha(\mathbf{x}_{g'}). \tag{5}$$

The particle force is interpolated by the same rules

$$\mathbf{A}_\alpha(x_j, t) = \left(\frac{q}{m}\right)_\alpha \sum_g i(\mathbf{x}_j - \mathbf{x}_g)\, H^*\mathbf{E}(t), \tag{6a}$$

$$H^*\mathbf{E}(t) = \sum_{g'} h(\mathbf{x}_g - \mathbf{x}_{g'})\, \mathbf{E}(\mathbf{x}_{g'}, t), \tag{6b}$$

so that particle self-force is avoided.

The interpolation function i may be chosen in many ways. For example, i may be chosen to give a subtracted dipole [14] expansion of h. However, the implicit time differencing algorithm adopted below requires derivatives of h to be computed. Thus, i is typically chosen to be at least once differentiable. Linear or quadratic splines [15] have been used for i to obtain the numerical results of Section IV.

To obtain the appropriate equations for low-frequency simulation, Eqs. (1)–(3) are normalized and differenced in time. Normalized variables (denoted by carats) are defined in the conventional way as: $\hat{\mathbf{x}}_j = \mathbf{x}_j/\Delta$; $\hat{\mathbf{v}}_j = \mathbf{v}_j\,\Delta t/\Delta$; $\hat{\mathbf{A}}_e = \nabla\hat{\phi}$; $\hat{\mathbf{A}}_i = -(m_e/m_i)\,\hat{\mathbf{A}}_e$; $\hat{\phi} = (e/m_e)(\Delta t/\Delta)^2\, H^*\phi$; $\hat{\rho} = (1/n_0 e)(N_0/N_x N_y)\rho$; $\hat{n}_\alpha = (1/n_0)(N_0/N_x N_y)\, n_\alpha$; $\hat{\nabla} = \Delta\nabla$; $\hat{\nabla}^2 = \Delta^2\nabla^2$; $\hat{t} = \omega_{e0} t$; $\Delta\hat{t} = \omega_{e0}\,\Delta t$; $\hat{\mathbf{\Omega}}_\alpha = \mathbf{\Omega}_\alpha\,\Delta t$; where Δ is the size of the N_x by N_y cells and Δt the time step of the simulation, and where n_0 is the mean electron density of the plasma with associated plasma frequency ω_{e0}.

Denoting time levels by superscripts, the normalized difference equations corresponding to Eq. (1) are written as a modified leap-frog scheme. Dropping the carats henceforth for notational convenience,

$$\mathbf{x}_j^{n+1} = \mathbf{x}_j^n + \mathbf{v}_j^{n+1/2}, \tag{7a}$$

$$\mathbf{v}_j^{n+1/2} = \mathbf{v}_j^{n-1/2} + \bar{\mathbf{A}}_\alpha^n(\mathbf{x}_j^n) + \mathbf{v}_j^{n+\gamma} \times \mathbf{\Omega}_\alpha, \tag{7b}$$

where the exact definitions of $\bar{\mathbf{A}}_\alpha^n$ and $\mathbf{v}_j^{n+\gamma}$ are yet to be given.

The field Eqs. (3)–(5) become

$$\nabla^2\phi^n = \Delta t^2\, \frac{N_x N_y}{N_0}\, H^2{}^*(n_e^n - n_i^n), \tag{8}$$

where $H^2{}^*$ has been written for H^*H^*.

b. *Decentered Equations for $\Omega_\alpha \gg 1$*

Consider first the last term in Eq. (7b). Let $\mathbf{v}^{n+\gamma}$ be defined by linear interpolation,

$$\mathbf{v}^{n+\gamma} = (\tfrac{1}{2} + \gamma)\, \mathbf{v}^{n+1/2} + (\tfrac{1}{2} - \gamma)\, \mathbf{v}^{n-1/2}. \tag{9}$$

For $\gamma = 0$ (and $\bar{\mathbf{A}}_\alpha^n = \mathbf{A}_\alpha^n$), Eq. (7b) becomes the usual time centered Lorentz force equation for advancing particle data [16, 17]. This difference scheme is absolutely stable and second-order accurate for $\Omega_\alpha \lesssim 1$.

For $\Omega_\alpha \gg 1$, Eq. (7) no longer correctly represents gyromotion. Rather, the cyclotron frequency aliases to the Nyquist frequency, $\omega_0 = \pi/\Delta t$, and the orbit

degenerates to two positions alternately assumed on alternate time steps. In this case, $\gamma > 0$ is chosen to damp this aliased motion by decentering the difference equations. All effects of gyration are then eliminated from the model, and, as is shown below, Eq. (7) describes the motion of the zero gyroradius guiding center. It is straightforward to include finite gyroradius effects by adding additional forces to Eq. (7) and simultaneously modifying the charge-current source equations [10, 13, 18]. Such an extension of the present work will be described in a future publication.

For low-frequency phenomena ($\mathbf{A}_\alpha(\cdot, t)$ slowly varying), Eq. (7) becomes a difference approximation to the Lorentz force equation. Northrup [19] has shown that this differential equation describes the motion of a guiding center when appropriate gyroaveraged forces are included on the right. The drift motions retained when these additional forces are omitted are those which persist at zero gyroradius. These are the electric drift and the inertial drifts; of which the two most significant are the centrifugal and polarization drifts.

The effect of introducing damping for $\gamma > 0$ is to select that solution of the differential equation which corresponds to the initial conditions appropriate for the drift motion solution [18, 19]. Low-frequency motion is little affected by this damping and, while the resulting difference approximation is formally only first-order accurate for $\gamma > 0$, γ may be chosen so small that second-order accuracy is effectively attained.

Indeed, expanding $\mathbf{v}$ in a Taylor series in t, Eqs. (7) and (9) give a differential equation whose solution for $\Omega_\alpha \gg 1$ is

$$\mathbf{v}_\perp = \frac{\mathbf{E} \times \mathbf{B}}{B^2} + \frac{m\dot{\mathbf{E}}_\perp}{qB^2} - \gamma \Delta t \frac{d}{dt}\left[\frac{\mathbf{E} \times \mathbf{B}}{B^2} + 2\frac{m\dot{\mathbf{E}}_\perp}{qB^2}\right] + O(\Delta t^2), \tag{10a}$$

$$\dot{v}_\parallel = \frac{q}{m} E_\parallel + O(\Delta t^2). \tag{10b}$$

Thus second-order accuracy is attained for modes such that

$$\gamma \lesssim |\omega| \Delta t < 1. \tag{11}$$

As the results of Section III confirm, γ may be chosen very small (typically $\gamma \sim 10^{-1}$) so that the condition of Eq. (11) is easily satisfied.

The decentered method described here may thus be applied when $\Omega_\alpha \gg 1$ with $\gamma > 0$ (the case of most interest in magnetic fusion). If $\Omega_\alpha \ll 1$, $\gamma = 0$ gives second-order accurate leap-frog equations for following the actual particle gyromotion. One of these conditions must hold uniformly in the simulation domain. That is, the efficient simulation of geometries in which Ω_α varies widely is not possible using the algorithm described here.

c. *Predictor–Corrector Method for* $\omega_\alpha \gg 1$

Consider next the electric acceleration term on the right of Eq. (7b). This term

represents the self-consistent collective interaction of all simulation particles through the Maxwell Eqs. (3). It is useful to replace this complicated interaction by a simplified model problem so that the implicit time differencing scheme is developed in a more transparent manner. Accordingly, Eq. (7) is replaced by the harmonic oscillator system

$$x^{n+1} = x^n + v^{n+1/2}, \tag{7a'}$$

$$v^{n+1/2} = v^{n-1/2} - \omega_m^2 \bar{x}^n, \tag{7b'}$$

where ω_m is the (true) mode frequency (times Δt) and the super bar represents an, as yet unspecified, combination of various time levels of x^n.

For low-frequency plasma simulation, $\bar{x}^n$ should be chosen so that $\bar{x}^n \sim x^n$ for small frequencies but so that the usual stability condition $|\omega_m| \leqslant 2$ is avoided. In this way, desirable properties of the usual explicit leap-frog scheme ($\bar{x}^n = x^n$) are retained for the modes of interest. On the other hand, modes for which $\omega_m \to \infty$ (which are not representable on the time grid chosen) should be strongly damped and removed from the system. The optimum filtering of x^n to $\bar{x}^n$ would thus be such that $\bar{x}^n = x^n$ for $|\omega_m| < \omega_{\max}$ and such that the system response would be zero for $|\omega_m| > \omega_{\max}$.

This may be approximated by an implicit scheme in which $\bar{x}^n$ depends on time advanced information. Thus, $\bar{x}^n$ should depend on x^{n+1}. (It is shown below that this is necessary for stability as $\omega_m \to \infty$.) The desired filtering of x^n is accomplished by a linear filter with a finite number of poles [7]. Thus

$$\begin{aligned} &\bar{x}^n + \alpha_1 \bar{x}^{n-1} + \alpha_2 \bar{x}^{n-2} + \cdots + \alpha_{I-1} \bar{x}^{n-I+1} \\ &\quad = cx^{n+1} + \beta_0 x^n + \beta_1 x^{n-1} + \cdots + \beta_{J-1} x^{n-J+1}. \end{aligned} \tag{12}$$

To proceed Eqs. (7') and (12) are analyzed by the Z transform. It is assumed that $(x^n, v^{n+1/2}) = Z^n(x, v)$, where $Z = \exp(-i\omega \Delta t)$ and ω is the normal mode frequency of the difference system. The following dispersion relation results:

$$(Z-1)^2 + \omega_m^2 Z f(Z) = 0. \tag{13}$$

In Eq. (13), $f(Z)$ is the transfer function from x to $\bar{x}$. Suppose, without loss of generality, that $I = J$. Equation (13) becomes the polynomial equation

$$\begin{aligned} &(Z^{I-1} + \alpha_1 Z^{I-2} + \cdots + \alpha_{I-1})(Z-1)^2 \\ &\quad + \omega_m^2 Z(cZ^I + \beta_0 Z^{I-1} + \cdots + \beta_{I-1}) = 0. \end{aligned} \tag{14}$$

Inspection of Eq. (14) gives the requirements for the undetermined coefficients. For $\omega_m = 0$, there are $I+1$ roots and the α's must be chosen so the zeros of the first factor in Eq. (14) lie inside the unit circle.

As $\omega_m \to \infty$, there are $I+1$ roots at finite Z provided $c \neq 0$. If c vanishes, at least one of the root loci extends to ∞ and produces an unstable root for ω_m sufficiently large. Thus, $c \neq 0$ is necessary for stability at large ω_m.

For ω_m large, the roots are $Z = 0$ and the zeros of the last factor in Eq. (14). Choosing all β's $= 0$ causes all root loci to approach zero as $\omega_m \to \infty$ and produces the maximum desired damping of high-frequency modes.

Finally, for second-order accuracy at $\omega_m \sim 0$, $f \sim 1 + O(Z-1)^2$ as $Z \to 1$. These conditions imply that f may be written as

$$f(Z) = \frac{Z^I}{Z^I - (Z-1)^I + \alpha_1'(Z-1)^{I-1} + \cdots + \alpha_{I-2}'(Z-1)^2} \tag{15}$$

for $I \geqslant 2$, where the α_i' are such that all zeros of the denominator lie inside the unit circle. Indeed, it is clear that the transfer function of Eq. (15) satisfies all the above requirements and corresponds to a linear filter of the type given by Eq. (12).

The choice $I = 2$ gives the simplest zero parameter scheme [9] in which the bar operation on a quantity Q is given by

$$\bar{Q}^n = \tfrac{1}{2}(Q^{n+1} + \bar{Q}^{n-1}). \tag{$\bar{1}$}$$

For $I = 3$ there is one free parameter α_1'. Solution of the dispersion relation for finite ω_m shows that $\alpha_1' \leqslant -0.5$ is required for stability. The marginal case minimizes damping of low-frequency modes and gives the scheme

$$\bar{Q}^n = \tfrac{2}{5}(Q^{n+1} + 2\bar{Q}^{n-1} - \tfrac{1}{2}\bar{Q}^{n-2}). \tag{$\bar{2}$}$$

Schemes ($\bar{1}$) and ($\bar{2}$) are equivalent to the $D1$ and $D2$, respectively, schemes of Ref. [7] for the harmonic oscillator considered here. We return to the comparison of the present work with Ref. [7] at the end of this section.

The amplitude response of Eq. (7′) with $\bar{x}$ defined by schemes ($\bar{1}$) and ($\bar{2}$) are shown in Fig. 1. For comparison, the amplitude response of the simplest first-order (fully implicit) scheme ($\bar{x}^n = x^{n+1}$) is also shown. As can be seen, the damping at small ω_m is much reduced for either second-order scheme compared to the simplest first-order scheme. Note also that scheme ($\bar{2}$), with an additional pole introduced into the filter f, most nearly approximates the ideal step response described above.

When ($\bar{1}$) or ($\bar{2}$) is applied to the plasma-field simulation system given by Eqs. (7)–(8), a very large system of coupled difference equations result. It is impractical to solve such a large implicit system. Fortunately, it is only necessary to solve a much smaller system for the time filtered potential $\bar{\phi}^n$. Then the particles are advanced in time in a predictor–corrector iteration.

As discussed in the Introduction, field corrector equations may be obtained either by the implicit moment equation method [4, 5, 9] or by the direct method [6–8]. The derivation here follows the latter approach in which the mechanism for including finite sized particles becomes transparent. Similar derivations [10, 11] based on the moment equations leaves some indeterminancy in the inclusion of finite sized particle effects. As mentioned in Section IV, numerical results confirm the importance of consistently treating these effects as derived from the direct method.

In the predictor–corrector method, the particle equations are first solved with an

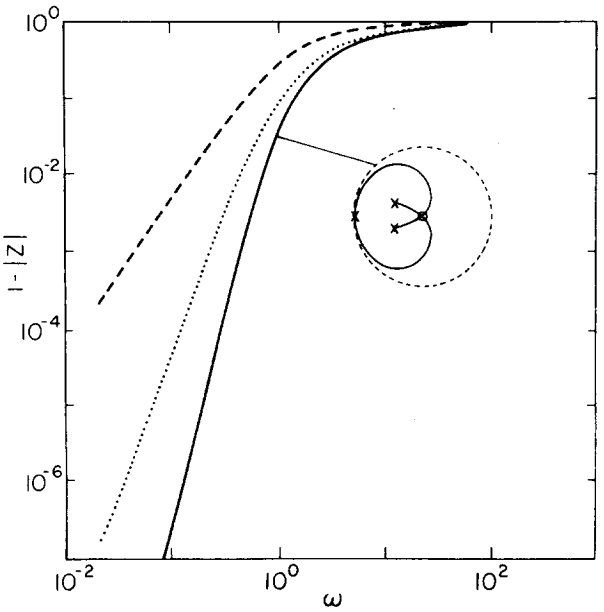

FIG. 1. Amplitude response for the harmonic oscillator problem with three different implicit difference schemes: (1), fully implicit-broken curve; (2) $\bar{1}$, dotted curve; (3) $\bar{2}$, solid curve. The abscissa is the normalized frequency of the system. The ordinate are closely related to the damping decrement. Also shown are the root loci for $\bar{2}$ relative to the unit circle. Two roots move from $Z = 1$ (marked by $\times$ on circle) to origin (0) as $0 \leqslant \omega \leqslant \infty$. The other two are strongly damped.

estimated $\bar{\phi}^n$. As described below, the first estimate of the potential is provided by $\bar{\phi}^n \sim \bar{\phi}^{n-1}$. Then the error in the field Eq. (8) is corrected by adjusting $\bar{\phi}^n$, taking account of the change in the right-hand side induced by a change in $\bar{\phi}^n$.

Denote a predictor–corrector iteration level by a superscript l written before. Then let ${}^l\bar{n}_\alpha^n$ be the raw densities resulting from pushing the particles with ${}^l\bar{\phi}^n$. That is,

$$ {}^l n_\alpha^{n+1} = \sum_{j\,\alpha} i(\mathbf{x}_g - {}^l\mathbf{x}_j^{n+1}), \tag{16} $$

with ${}^l\bar{n}_\alpha^n$ given from $(\bar{1})$ or $(\bar{2})$ with n_α^{n+1} replaced by the above estimate.

Associated with the lth iterate there is an error in Eq. (8)

$$ {}^l\varepsilon = \nabla^2 {}^l\bar{\phi}^n - \Delta t^2 \frac{N_x N_y}{N_0} H^2 * ({}^l\bar{n}_e^n - {}^l\bar{n}_i^n). \tag{17} $$

A correction to ${}^l\bar{\phi}^n$ is sought such that ${}^{l+1}\varepsilon \sim 0$.

Let δ denote first-order changes associated with $l \to l+1$, so that ${}^{l+1}\bar{\phi}^n \sim {}^l\bar{\phi}^n + \delta\phi$, etc. The change $\delta\varepsilon$ is computed to give a linear corrector equation from which $\delta\phi$ is determined. For this $\delta\bar{n}_\alpha$ is estimated from Eq. (16) using Eqs. (7) and (9).

For $\gamma \geqslant 0$, the solution of the difference Eqs. (7b) and (9) may be written as

$$\mathbf{v}_j^{n+1/2} = \vec{R}_\alpha \mathbf{v}_j^{n-1/2} + \vec{S}_\alpha \bar{\mathbf{A}}_\alpha^{n(\mathbf{x}_j^n)}. \tag{18}$$

The matrices $\vec{R}$ and $\vec{S}$ are given (in diadic notation) by

$$\vec{R}_\alpha = d_\alpha \{[1 - (1/4 - \gamma^2)\,\Omega_\alpha^2]\,\vec{I} - \boldsymbol{\Omega}_\alpha \times \vec{I} + (1/2 + \gamma)\,\boldsymbol{\Omega}_\alpha \boldsymbol{\Omega}_\alpha\}, \tag{19a}$$

$$\vec{S}_\alpha = d_\alpha \{\vec{I} - (1/2 + \gamma)\,\boldsymbol{\Omega}_\alpha \times \vec{I} + (1/2 + \gamma)^2\,\boldsymbol{\Omega}_\alpha \boldsymbol{\Omega}_\alpha\}, \tag{19b}$$

where

$$d_\alpha = \{1 + (1/2 + \gamma)^2\,\Omega_\alpha^2\}^{-1}, \tag{19c}$$

and $\vec{I}$ is the unit diadic.

From Eqs. (7a) and (18) the estimate

$$\delta^l \mathbf{x}_j^{n+1} = \delta^l \mathbf{v}_\alpha^{n+1/2} = \vec{S}_\alpha \frac{(q/m)_\alpha}{(q/m)_e} \nabla\, \delta\phi(\mathbf{x}_j^n)$$

is obtained. Thus, from Eq. (16),

$$\delta \bar{n}_\alpha = -\frac{(q/m)_\alpha}{(q/m)_e} f_n \nabla \cdot \vec{S}_\alpha \sum_{j\alpha} i(\mathbf{x}_g - {}^l\mathbf{x}_j^{n+1})\, \nabla\, \delta\phi(\mathbf{x}_j^n).$$

The field corrector is obtained from ${}^{l+1}\varepsilon \sim {}^l\varepsilon + \delta\varepsilon = 0$. Thus, $\delta\phi$ should satisfy

$$\nabla^2\, \delta\phi + \nabla \cdot H^2 * [\vec{S} \nabla\, \delta\phi] = -{}^l\varepsilon. \tag{20}$$

In the above $f_n = 1/2$ for $(\bar{1})$ and $2/5$ for $(\bar{2})$, and the matrix $\vec{S} = f_n \Delta t^2\, N_x N_y / N_0 \sum_\alpha {}^l n_\alpha^{n+1} \vec{S}_\alpha$. Also in Eq. (20) the last term has been approximated as

$$\begin{aligned}
&H^2 * \sum_{j\alpha} i(\mathbf{x}_g - {}^l\mathbf{x}_j^{n+1})\, \nabla\, \delta\phi(\mathbf{x}_j^n) \\
&\quad \sim \sum_{j\alpha} h_2(\mathbf{x}_g - {}^l\mathbf{x}_j^{n+1})\, \nabla\, \delta\phi(\mathbf{x}_j^n) \\
&\quad \sim \sum_{j\alpha} h_2(\mathbf{x}_g - {}^l\mathbf{x}_j^{n+1})\, \nabla\, \delta\phi({}^l\mathbf{x}_j^{n+1}) + O(kv) \\
&\quad \sim \sum_{g'} h_2(\mathbf{x}_g - \mathbf{x}_{g'})\, \nabla\, \delta\phi(\mathbf{x}_{g'}) \sum_{j\alpha} i(\mathbf{x}_{g'} - {}^l\mathbf{x}_j^{n+1}) \\
&\quad = H^2 * [{}^l n_\alpha^{n+1}\, \nabla\, \delta\phi],
\end{aligned}$$

where terms of order kv (k wavenumber) have been ignored and where the interpolation has been placed on the product of $h_2 \equiv H^* h$ and $\nabla\, \delta\phi$.

Note that the above approximation of the plasma response term leads to a field corrector very similar to that resulting from the moment equation method [4, 5]. In

fact, the success of the moment method is a major motivation for choosing this form of "simplified differencing" [8]. The moment equations specify no prescription for the treatment of the smoothing operator H resulting from the finite particle size. The derivation given here, based on simplifying the strict difference formulation of the direct method, gives the only form of the field corrector found to be consistent with finite sized particles. We return to this point in the next section where numerical results are given.

The neglect of the $O(kv)$ terms in Eq. (20) introduces a convergence condition for the predictor–corrector iteration which is found to be

$$k_{\max} \max \left\{ u, \frac{v_T}{\sqrt{2}} \right\} \leqslant 1, \tag{21}$$

for a nearly uniform plasma ($\omega_T \Delta t < 1$ where ω_T is the trapping frequency), where $k_{\max}$ is the maximum wavenumber of the system, u is the mean (fluid) velocity, and v_T the thermal velocity of the electrons.

The convergence condition of Eq. (21) is similar to that obtained by other authors [4, 5]. This time step constraint might be avoided by a more complex predictor–corrector iteration [8]. However, even if convergence were obtained for larger Δt, accuracy would be lost since many particles would travel a large fraction of a wavelength in a single time step. A possible technique for avoiding this constraint may be to combine implicit field methods of the type described here with orbit averaging techniques [20].

Many of the results of this subsection have been previously outlined or described by the Livermore group [6–8]. For example, schemes ($\bar{1}$) and ($\bar{2}$) of the present work are the same as the $D1$ and $D2$ schemes of Ref. [7]. The derivation is repeated here to make this paper more self-contained and to single out the specific algorithm used to obtain the results of Section III. The motivation for the derivation of ($\bar{1}$) and ($\bar{2}$) given here in terms of the linear filter of Eq. (12) may also be more satisfactory than that previously given.

Two important differences between the present work and the previous work should be emphasized. First, a particular simplified differencing scheme is adopted for the field corrector equation, so that numerical solution of Eq. (20) is convenient. The details of this differencing are given in the next subsection. Second, the recursive filter ($\bar{1}$) or ($\bar{2}$) is applied here to the mesh quantity ϕ rather than to the particle quantities **A**. This greatly reduces the storage requirements as well as the particle pushing time since the particle predictor and corrector pushes are done with explicit difference equations.

Because the filter is applied on the mesh, the difference scheme described above is not strictly momentum conservative. Thus moving particles suffer a drag self-force which is proportional to the square of their velocity. Numerically it is found that the effect of this force is extremely small since the bare particle drag is greatly reduced by collective shielding and since the constraint of Eq. (21) assures that the velocity of all particles is small.

Implicit time differencing methods of the type described here also introduce a sall amount of damping of the collective plasma modes, as seen above for the harmonic oscillator system. This damping is observed to lead to (primarily electron) cooling in implicit simulations [5, 7, 8, 13]. Because the difference equations described here are second-order accurate at low frequencies and because the damping associated with either $(\bar{1})$ or $(\bar{2})$ is extremely small except at the highest realizable frequencies, this cooling rate is very low for reasonable simulation parameters and is not a significant limitation on the applicability of the method. This is confirmed by the numerical results of Section III below.

A more worrisome aspect of the numerically introduced dissipation is the possibility of destabilization of negative-energy modes. Langdon [21] has pointed out that dissipation combined with the lack of Galilean invariance in the non-momentum conservative scheme described here can, for instance, destabilize the slow space charge wave for a cold, drifting electron beam. As shown in Ref. [7], this instability is avoided in Galilean invariant schemes, since, without differential motion of the particles, there is no possibility for dissipation.

However, as shown in the Appendix, this instability is stabilized again in the present scheme in the regime of most interest, i.e., for *large* enough time steps. The lower bound on Δt depends on the drift velocity, but all modes become stable in a cold, drifting electron plasma for $\Delta t \geqslant 2$. In fact, the stability condition (A10) is easily satisfied in the application of low-frequency methods of the type described here. In dimensionless variables Eq. (A10) becomes $(k\lambda_D)(u/v_T) \leqslant 1$, where λ_D is the electron Debye length, and where Eq. (21) has been used to expand for small ku. Since low-frequency phenomena are characterized by long wavelength and small drift velocities, both factors above are small and stability is easily maintained.

d. *Iteration Method*

To complete the predictor–corrector iteration scheme, Eq. (20) must be solved for $\delta\phi$. For a non-constant density plasma, this equation is a differential-integral elliptic equation with variable coefficients. The direct inversion of Eq. (19) used in one-dimensional applications [4–8] is not efficient in two or more dimensions. The most appropriate solution schemes for such a multi-dimensional problem are iterative refinement methods in which an approximate inverse is applied to the residual to obtain a correction, in turn reducing the residual.

An effective method of this type is obtained by writing Eq. (20) in $\mathbf{k}$ space and "renormalizing" [10]. The Fourier transform of Eq. (20) is

$$k^2\,\delta\phi(\mathbf{k}) + |h(\mathbf{k})|^2 \sum_{\mathbf{k}'} \mathbf{k}\cdot\vec{S}(\mathbf{k}-\mathbf{k}')\cdot\mathbf{k}'\,\delta\phi(\mathbf{k}') = {}^{l}\varepsilon(\mathbf{k}). \tag{22}$$

The convolution sum over $\mathbf{k}'$ represents the interaction of all $\mathbf{k}'$ modes with the $\mathbf{k}$ mode through the density fluctuations contained in S. This sum may be decomposed into a "self-interaction" part representing the coupling of a $\mathbf{k}'$ mode to itself ($\mathbf{k} = \mathbf{k}'$), and a "mode-coupling" part ($\mathbf{k} \neq \mathbf{k}'$).

In the spirit of weak turbulence theory, it is natural to renormalize the free space dielectric (first term of Eq. (22)) by including the self-interaction term in an approximate inverse and considering the mode coupling terms as smaller. An inner iteration (indicated by a superscript m below) to solve Eq. (20) is obtained by this approach as

$$ {}^{m+1}\delta\phi(\mathbf{k}) = \frac{{}^{l}\varepsilon - |h(\mathbf{k})|^2 \sum_{\mathbf{k}' \neq \mathbf{k}} \mathbf{k} \cdot S(\mathbf{k}-\mathbf{k}') \cdot \mathbf{k}' \, {}^{m}\delta\phi(\mathbf{k}')}{k^2 + |h(\mathbf{k})|^2 \mathbf{k} \cdot \bar{S}(0) \cdot \mathbf{k}}. \tag{23} $$

It is easily verified that the above approach amounts to constructing an approximate inverse by replacing the variable susceptibility represented by S by its average value over the entire computational domain. This iterative method is closely related so that employed in magnetoinductive or Darwin simulation models [22]. The convergence properties of such global iterations have been discussed by Concus and Golub [23]. The iteration of Eq. (23), however, is not strictly of the type considered in Ref. [23], since the residual operator contains first derivatives on the solution, nor is the transformation of Ref. [23] for the analagous scalar equation applicable to the tensor field corrector of Eq. (20).

Thus, although the convergence of Eq. (23) to the desired solution cannot be guaranteed for all density profiles, very rapid convergence is to be expected for a nearly uniform plasma. As seen from the numerical results of Section III, this is indeed the case. In fact, even for radically non-uniform plasmas, the iteration of Eq. (23) is found to converge in a few steps to the necessary accuracy, indicating a broad applicability of this method.

In implementing the iteration of (23), a combination of $\mathbf{r}$ and $\mathbf{k}$ space operations are used to conveniently evaluate the convolution sums. Let ${}^{m}\xi = {}^{m+1}\delta\phi - {}^{m}\delta\phi$. Equation (23) may be rewritten as

$$ {}^{m}\xi(\mathbf{k}) = \frac{{}^{m}s(\mathbf{k})}{k^2 + |h(\mathbf{k})|^2 \mathbf{k} \cdot \bar{S}(0) \cdot \mathbf{k}}, \tag{24} $$

where the residual ${}^{m}s$ is the difference of the right-hand and left-hand sides of Eq. (22) with ${}^{m}\delta\phi$ used for $\delta\phi$.

It is straightforward to verify the following procedure which is used to iterate Eq. (23). For $m = 1$, ${}^{1}s = {}^{l}\varepsilon$, $\delta\phi = 0$. For $m \to m+1$, obtain ${}^{m}\xi$ from Eq. (24), then ${}^{m+1}\delta\phi = {}^{m}\delta\phi + {}^{m}\xi$. Multiply ${}^{m}\xi$ by $i\mathbf{k}$ and inverse Fourier transform to $\mathbf{r}$ space. Multiply the resulting vector by $S(\mathbf{r})$ and transform back to $\mathbf{k}$ space. Multiply this result by $i|h(\mathbf{k})|^2\mathbf{k}\cdot$ and add to ${}^{m}s(\mathbf{k})$. Finally, subtract $k^2 {}^{m}\xi$ from this result to obtain ${}^{m+1}s(\mathbf{k})$. Repeat until $\max\{|{}^{m}s(\mathbf{k})|\}$ satisfies a specified convergence criterion.

III. Simulation Results

In this section, the general properties of the model are investigated in two simple physical systems using a simulation code based on the low-frequency model of Section II. In the first case, the ion-acoustic fluctuations of a uniform, thermal, unmagnetized, two-temperature, one-dimensional plasma are examined. Since the ion-acoustic fluctuations represent an extremely small part of the total fluctuation energy of a thermal plasma and are strongly affected by electron Landau damping in the parameter range studied, these results represent a severe test of the applicability of the model.

In the second case, a very strongly non-uniform plasma is examined. A two-dimensional plasma is suspended against a gravitational force by a magnetic field normal to the plane of simulation. The initial density profile is such that the plasma density is nearly uniform in the left half of the simulation domain, and nearly zero in the right half. An unstable gravitational interchange is observed for parameters such that the growth rate is five orders of magnitude lower than the electron plasma or cyclotron frequencies.

In both cases, the second-order accurate scheme ($\bar{2}$) has been used and quadratic splines have been used to interpolate the charge density from and the force to the particles. The fluctuation spectrum was observed using a one-dimensional, unmagnetized version of the algorithm described above. Simulation parameters were (recall that normalization is such that $\Delta = 1$, $\omega_e = 1$); (system length) $N_x = 128$, (number of particles) $N_0 = 9216$, (particle size) $a = 3$, where the Gaussian particle shape is given by $h = \exp\{-1/2a^2\delta^2\}$.

The thermal velocity of the electrons is such that $v_T = 0.05$, so that the electron Debye length $\lambda_D = 0.05$. The ion-to-electron mass ratio is $m_i/m_e = 100$, while the electron-to-ion temperature ratio is $T_e/T_i = 20$. Electrons and ions are loaded uniformly on the spatial mesh at $t = 0$ and given Maxwellian velocity distributions for this thermal run. The time step is fixed at $\Delta t = 10$, a factor of 50–100 increase over that allowed for an explicit code in which ω_e has to be resolved. The calculation comprises 16,384 time steps or $163{,}840\omega_e^{-1}$ so that many ion-acoustic wave periods are resolved. Since the plasma is nearly uniform, the iterative solution of Eq. (23) requires only two iterations to converge to a relative error of 10^{-5} of the equivalent mean density. No iteration of the particle pushing beyond the first correction has been deemed necessary.

A short digression is appropriate here to discuss some observations which led to the choice of these parameters and which bear on the applicability of implicit methods in general. In addition to the large time step employed, two other simulation parameters contrast sharply to those appropriate for explicit simulation. First, the particle size is much larger than that which is optimum for explicit calculations (typically, $a = 1$ there). Other tests have shown that stability is improved and cooling is reduced as the particle size is increased from $a = 1$, with a threshold of $a = 2$ for tolerable cooling. For smaller values of a, performance is somewhat improved when quadratic splines are used compared to that obtained using linear splines or multipole

expansion. However, acceptable performance still requires $a \gtrsim 2$. For $a = 3$, as in the simulations described here, there is very little dependence of the results on whether SUDS, linear splines, or quadratic splines are used to interpolate the finite sized particles. The cooling rate is also found to be reduced to a much smaller extent when either the number of particles per cell, the time step, the system length, or any combination of these is increased at constant particle size.

A second contrast occurs in the choice of v_T and associated $\lambda_D \ll 1$. This is required by condition (21), which is essentially a Courant–Friedrich–Lewy condition on the time step. In contrast to explicit methods, however, $\lambda_D \ll 1$ does not lead to severe finite grid instabilities since the plasma oscillation branch is removed for $\Delta t \gg 1$. Thus, implicit methods are appropriate for studying long-wavelength modes in a large system. (Quasi-neutral algorithms [24] also share this property but omit all electron kinetic effects.)

Several additional interesting points can be seen from tests cases other than the ones reported here in detail. First, the form of the field corrector, Eq. (20) is found to be the only one consistent with finite sized particles. If, for example, the smoothing operator, H^2*, is applied to either or both of S and $\nabla \delta\phi$ before their product is taken, severe electron cooling, heating, or instability of the algorithm is observed. The direct method gives the correct form [8] (modulo simplifying the differencing as indicated in Section IIc). The moment method leaves indeterminate the form of the corresponding terms. If these terms are interpreted as in Eq. (20), the results of the moment method and the direct method are essentially identical.

Second, the reduction in cooling obtained for the second-order accurate methods described here compared to a fully implicit first-order accurate method is not as dramatic as the reduction in low frequency mode damping (see Fig. 1). For the parameters described above, the cooling rate is only reduced by a factor of 2 for the second-order accurate method (in one-dimensional geometry). It appears that cooling is due to the following phenomenon. Fast electrons with velocities v_j excite ballistic modes with frequency $\omega = kv_j$ much larger than the collective mode frequency kc_s. These higher frequency modes suffer larger numerical damping than the collective modes and their damping seems to be the major cause of the cooling. The higher order accurate method is used here and in other applications to improve the fidelity of low-frequency response (reduced damping) at no increase in computational complexity.

Returning to the ion-acoustic simulation described previously, the time evolution of electron and ion temperatures, normalized to their initial values, are shown in Fig. 2a. The temperature is measured as $\langle v^2 \rangle - \langle v \rangle^2$, the average being taken over all N_0 particles of either electron or ion species. The total momentum, proportional to $\langle v \rangle$ remains less than 10^{-5} of the velocity associated with the above temperature; thus, the temperatures also measure the total kinetic energies. The time evolution of the total energy, normalized to its initial value, is shown in Fig. 2b. The ion temperature increases by 55%, while the electrons cool by 20%. Total energy decreases by only 12% over $163{,}840\omega_e^{-1}$. The electrostatic energy is essentially constant throughout the calculation. In this case, the plasma parameter (ratio of average Coulomb energy to

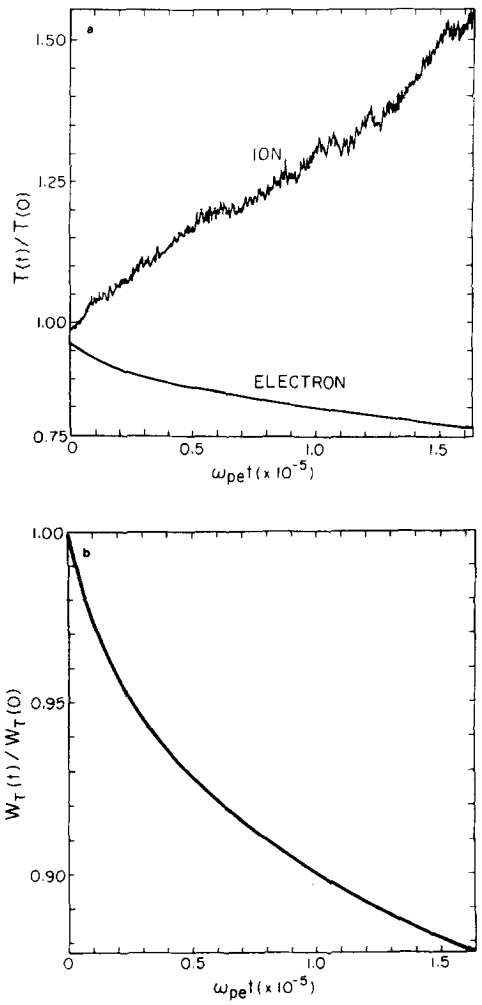

FIG. 2. (a) Electron and ion temperatures normalized to their $t = 0$ values as a function of time. (b) Total energy normalized to its $t = 0$ value as a function of time.

initial kinetic energy) is $g \simeq 2 \times 10^{-3}$. Electron cooling, which causes the total energy decrease is due to the numerical damping discussed in the previous section. Local velocity space diagnostics show that the fast or tail electrons are the ones that are slowing down most rapidly. The ion heating is physical and due to ion Landau damping of the ion-acoustic waves.

The collective behavior of the plasma at frequencies $\omega \ll \omega_e$ is displayed in Figs. 3a and b. The time averaged electrostatic energy per wavenumber, $\langle E_k^2/8\pi \rangle$, normalized to the thermal energy per degree of freedom, $k_B T_e/2$ (k_B is Boltzmann's constant), or fluctuation spectrum is shown in Fig. 3a. The ion-acoustic frequency

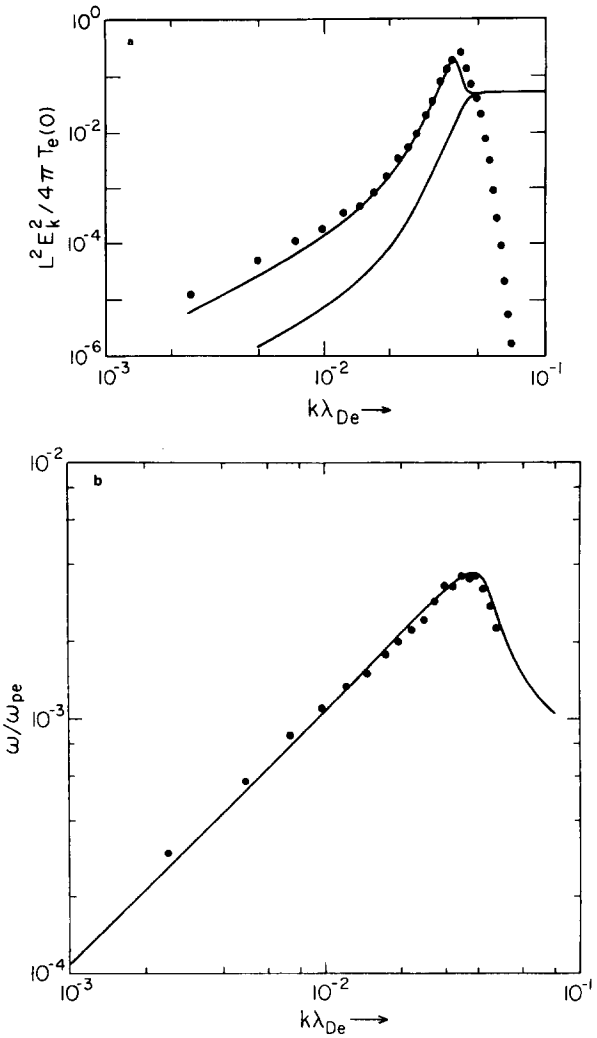

FIG. 3. (a) Fluctuation spectrum for thermal plasma. Normalized electrostatic field energy as a function of wavenumber is shown. Upper curve is theory including electron Landau damping; lower theory neglecting electron Landau damping; points are simulation results. (b) Frequency spectrum for thermal plasma. Normalized frequency versus normalized wavenumber is plotted. Curve is theory; points are simulation results.

spectrum, normalized frequency, ω/ω_e, versus normalized wavenumber, $k\lambda_D$, is shown in Fig. 3b.

For $T_e \gg T_i$, and $\omega \ll \omega_e$, the fluctuation spectrum of a two-temperature Maxwellian plasma can be written as [25]

$$\frac{\langle E_k^2/8\pi\rangle}{k_B T_e/2} = \frac{T_i}{T_e}\frac{k^2\lambda_D^2|h(k)|^2}{1+k^2\lambda_D^2|h(k)|^2}\cdot\left\{\frac{\Theta+[(m_e/m_i)(T_i/T_e)]^{1/2}}{\Theta+(m_e/m_i)^{1/2}(T_i/T_e)^{3/2}}\right\}, \tag{25}$$

where

$$\Theta = \exp\left\{-\frac{T_e/2T_i}{1 + k^2\lambda_D^2 |h(k)|^2}\right\}. \tag{26}$$

The first term on the right-hand side of Eq. (25) is the term one obtains if the electrons are treated adiabatically as in quasi-neutral simulations. Its multiplier represents the contribution of ion and electron Landau damping to the fluctuation energy from resonant ions and electrons. For $T_e \gg T_i$ the second term in the multiplier dominates over Θ and the normalized fluctuation energy approaches $k^2\lambda_D^2 |h(k)|^2/(1 + k^2\lambda_D^2 |h(k)|^2)$.

A stringent test of the electron response at low frequencies is afforded by comparison of the simulation results with the prediction of Eq. (25). If resonant electron response is retained by the implicit method, the fluctuation spectrum will obey Eq. (25). If the low-frequency electron response is essentially adiabatic, the fluctuation spectrum will closely follow only the first term on the right of Eq. (25). A simulation using the quasi-neutral simulation model [24] indeed verifies the latter scaling.

In Fig. 3a the fluctuation spectra predicted by Eq. (25) and that predicted for adiabatic electrons are plotted in the upper and lower solid curves, respectively. The ratio of the former to the latter is approximately T_e/T_i. The simulation fluctuation spectrum indicated by dots closely follows the prediction of Eq. (25). Note also that the wavenumbers with maximum energy observed in the simulation and predicted by theory agree exactly. At larger wavenumbers, the theory is questionable because of approximations made in the derivation of Eq. (25). The effect of the previously mentioned ballistic electron modes on the fluctuation spectrum is to increase its intensity above the theoretical level Eq. (25). When most of the noise due to these ballistic modes is suppressed by frequency filtering, as in Fig. 3a, where a filter of width $\Delta\omega = 0.02\omega_e$ about $\omega = kc_s$ is used, the intensity of the spectrum decreases, but its shape is preserved, and closer agreement with theory results. Since this extra ballistic noise is due to particle discreteness, increasing the number of particles further reduces the discrepancy.

In summary, the fluctuation spectrum indicates that the resonant electron response at low frequencies is described accurately by the implicit method described here. It is also clear from these results that fluctuations at mode frequencies higher than the ion-acoustic range have been suppressed; otherwise the spectrum would have obeyed the usual scaling $1/(1 + k^2\lambda_D^2 |h(k)|^2)$.

The theoretical ion-acoustic dispersion relation, ω/ω_e versus $k\lambda_D$, obtained from a numerical solution including finite grid effects is shown as a solid curve in Fig. 3b. The measured simulation frequencies, shown by dots in that figure, are in excellent agreement with the theory. No higher mode frequencies were observed in the spectrum. A very low intensity tail due to the ballistic electron modes is seen extending beyond the ion-acoustic frequency. These one-dimensional results clearly demonstrate the efficacy of the implicit method described here for studying low-

frequency phenomena in a thermal plasma. Next, a two-dimensional, magnetized plasma is examined using these methods.

An unstable gravitational interchange is studied in two dimensions for an inhomogeneous plasma. This calculation is carried out for (system size) $N_x = N_y = 32$, (number of electrons or ions) $N_0 = 4608$, (mass ratio) $m_i/m_e = 100$, (electron cyclotron frequency) $\Omega_e = 1$, and (particle size) $a = 3$. The magnetic field is normal to the plane of simulation.

Electrons and ions are loaded initially with their guiding center velocity ($\mathbf{v}_\perp = 0$) in such a way that the distribution of particles is uniform in the left half of the simulation domain. No particles are loaded in the right half of the domain. A gravitational acceleration to the right drives an unstable interchange localized near the interface at the middle of the domain.

The perturbed potential ψ for such an interchange satisfies the differential equation [26]

$$\frac{d}{dx}\left(1+\frac{\omega_i^2}{\Omega_i^2}\right)\frac{d\psi}{dx} - k_y^2\left(1+\frac{\omega_i^2}{\Omega_i^2}\right)\psi + \frac{k_y^2 g}{\omega^2\Omega_i^2}\frac{d\omega_i^2}{dx}\psi = 0, \tag{27}$$

where g is the gravitational acceleration. For the sharp density gradient case considered here, the above reduces to the algebraic condition

$$\omega^2 = -\frac{|k_y| g}{1 + 2\Omega_i^2/\omega_i^2}. \tag{28}$$

In Eqs. (27) and (28), the effect of the polarization motion of the ions is very important for high density plasmas ($\omega_i/\Omega_i \gg 1$). If the polarization motion is neglected, the first term in the denominator of Eq. (28) is omitted and the growth rate

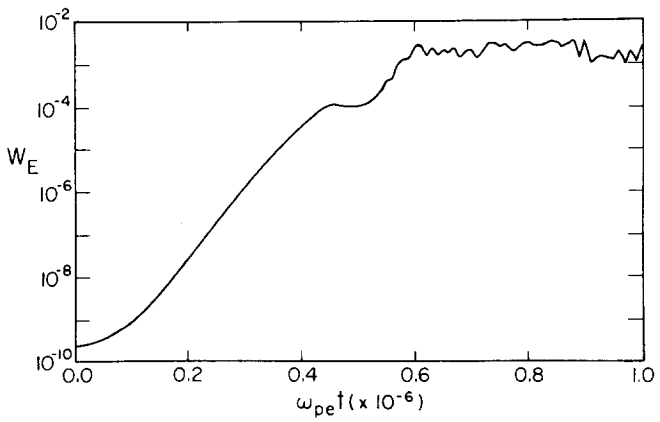

FIG. 4. Electrostatic field energy (normalized units) as a function of time for unstable gravitational interchange.

becomes unphysically large for the high density case. For the simulation parameters considered here, $\omega_i/\Omega_i = 10$, so the physical growth rate $\gamma \simeq \sqrt{|k_y| g}$, while the growth rate neglecting polarization is ~ 7 times larger.

In the simulation, iteration of Eq. (23) is used to obtain the field corrector with extremely large $\Delta t = 10^3$. Convergence to 10^{-8} of the equivalent mean density requires between 1 and 20 iterations, the latter number being required only briefly during the strongly nonlinear phase of the simulation.

The simulation results for $g = 2 \times 10^{-9}$ are summarized in Figs. 4 and 5. In this case the plasma is initially perturbed with the longest y wavelength, $k_y = 2\pi/N_y$, so

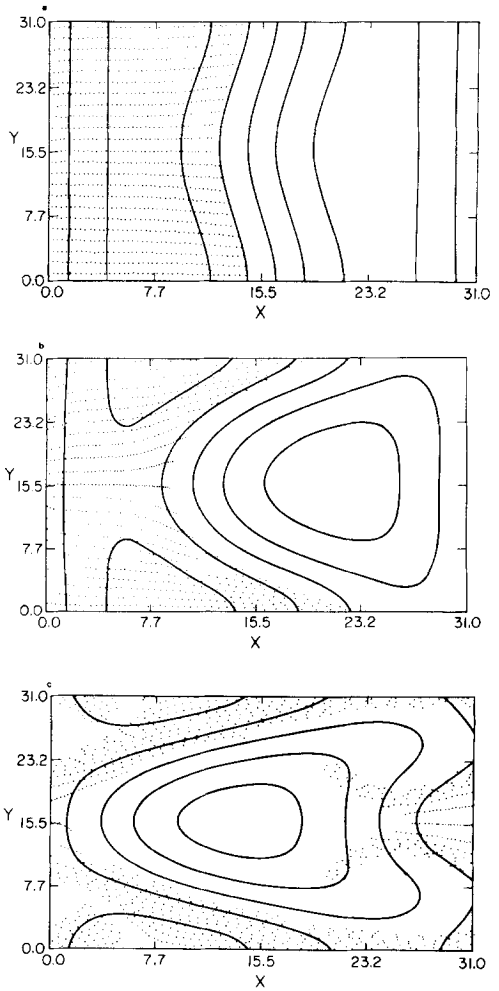

FIG. 5. Snapshots of finite size ion density contours are shown along with point plot of ion positions for three times near saturation of gravitational interchange. (a) $\omega_e \Delta t = 3 \times 10^5$; (b) $\omega_e \Delta t = 4 \times 10^5$; (c) $\omega_e \Delta t = 5 \times 10^5$.

that the growth rate of a single mode may be more accurately measured. With only noise as the initial perturbation, several long y wavelength modes grow simultaneously with nearly equal growth rates. A value of 0.1 was selected for the decentering parameter γ of Eqs. (7) and (9) to optimize code performance. In Fig. 4, the electrostatic field energy is shown in a semi-log plot as a function of time. The growth rate of $\gamma = 2.4 \times 10^{-5}$ determined from $W_E = W_E(0) \exp\{2\gamma t\}$ is in good agreement with the theoretically predicted value of $\gamma = 2.7 \times 10^{-5}$, verifying the correct modelling of ion polarization motion.

Figure 5 shows three different snapshots of the finite particle size ion density contours. The positions of roughly 10^3 of the ions are also shown as points in the figure. As can be seen, the unstable interface near the middle of the simulation domain evolves through a linear growth stage, toward a nonlinear "spike and bubble" stage. The only saturation mechanism is provided by the finite size of the periodic simulation boundary. Thus, plasma leaving on the right (left) reenters on the left (right). In this way the configuration evolves toward a state of nearly steady flow with constant potential driving stationary vortices.

The simulation results presented in this section demonstrate the accuracy and efficacy of the methods described here when applied to the study of low-frequency, magnetized plasma phenomena.

IV. Conclusions

The second-order accurate simulation method described here is appropriate for the study of low-frequency phenomena in a magnetized plasma. A field corrector derived by the direct method (with differencing simplified) correctly treats finite sized particles. The guiding center motion of both ions and electrons is accurately followed for $\Omega_\alpha \gg 1$ by a simple decentered differencing of the Lorentz force particle pushing equations. A straightforward iteration of the field corrector is developed based on the renormalized plasma simulation method.

Numerical results confirm reduced electron cooling for the second-order accurate method. The numerical experiments also show that finite particle size may only be incorporated in an implicit calculation as indicated by the direct method derivation. The efficiency of the iterative method for solving the field corrector is demonstrated for both nearly uniform and strongly inhomogeneous plasmas.

Accurate numerical results are obtained in two stringent test cases. First, the ion-acoustic fluctuations of a thermal plasma demonstrate the accuracy with which kinetic electron effects on low-frequency oscillations are represented. Second, the simulation of an unstable gravitational interchange in a sharp density gradient plasma, demonstrates the applicability of the method to nonlinear phenomena at extremely low frequencies (growth rate $\gamma \simeq 10^{-5}\omega_e$).

The method described here may be easily extended in three directions. First, gyroaverage forces may be added to the Lorentz force and gyroaveraged sources to the field equations to represent finite ion gyroradius effects. Second, the simulation

may be made fully electromagnetic by the addition of a nearly explicit time advance of the vector potential. Third, the simulation geometry may be readily changed to represent more realistic configurations with more realistic boundary conditions. Many of these extensions have been outlined in the references and details will be presented in future publications.

Appendix: Dispersion Relation for Cold Drifting Electron Plasma

In this appendix the dispersion relation for a cold, drifting electron beam is derived and conditions for stability are discussed. A small perturbation about a uniform, field-free, one-dimensional equilibrium is assumed. First, the perturbed particle orbits are computed from the difference Eqs. (7). Next, the perturbation in the particle positions are used to compute the density perturbation [3]. Finally, the density perturbations are used to obtain the dispersion relation from the field Eq. (8). The derivation follows standard methods and details are omitted.

Let Z be as in Section IIc, and denote by $f(Z)$ the transfer function associated with

$$f_1(Z) = \frac{Z^2}{2Z - 1} \tag{A1}$$

$$f_2(Z) = \frac{Z^3}{5/2Z - 2Z + 1/2}. \tag{A2}$$

Let u be the (normalized) drift velocity of the cold electrons. The dispersion relation for the scheme $(\bar{1})$ or $(\bar{2})$ with the filtering applied on the mesh as discussed in Section IIc is

$$1 + \Delta t^2 f_i(Z) \frac{W}{(W-1)^2} = 0, \tag{A3}$$

where

$$W = Ze^{iku}, \tag{A4}$$

and the finite size particle effects have been neglected.

For Δt small this dispersion relation predicts instability of the slow ($\omega \sim ku - \omega_e$) space charge wave [19]. For sufficiently large Δt, however, all roots of Eq. (A3) become stable. To show this, examine Eq. (A3) for Δt such that $Z \sim 1$. Putting $Z = 1$ gives the marginal time step

$$\Delta t_0 = 2 \sin \tfrac{1}{2} ku. \tag{A5}$$

Expanding $\Delta t = \Delta t_0 + \tau$, $Z = 1 + \sum_j Z_j \tau^j$ for $\tau/\Delta t_0 \ll 1$ determines Z_j order by order. After some tedious algebra there results

$$Z \sim 1 + iS\tau - S^2(\tfrac{1}{2} + \tfrac{3}{4}T)\,\tau^2 - (\tfrac{1}{4}S^3T + iI_1)\,\tau^3 + O(\tau^4), \tag{A6}$$

for $(\bar{1})$, and

$$\begin{aligned} Z \sim 1 &+ iS\tau - S^2(\tfrac{1}{2} + \tfrac{1}{4}T)\,\tau^2 + S^3[\tfrac{1}{4}T - i(\tfrac{3}{2} - \tfrac{1}{2}T^2)]\,\tau^3 \\ &+ S^4[\tfrac{1}{4} - \tfrac{5}{32}T^2 + iT(\tfrac{3}{64} - \tfrac{5}{64}T^2)]\,\tau^4 \\ &- [S^5T(\tfrac{11}{8} + \tfrac{9}{64}T^2) + iI_2]\,\tau^5 + O(\tau^6) \end{aligned} \tag{A7}$$

for $(\bar{2})$. In Eqs. (A6)–(7), $S = \sec ku/2$, $T = \tan ku/2$, and I_1, I_2 are real numbers independent of τ.

The condition for stability for $\Delta t \sim \Delta t_0$ is found from $1 \geqslant |Z^2|$. From (A6)–(A7) follows

$$|Z^2| \sim 1 - 2S^3T\tau^3 + O(\tau^4), \tag{A8}$$

for $(\bar{1})$, and

$$|Z^2| \sim 1 - S^5T(\tfrac{55}{32} + \tfrac{3}{16}T^2)\,\tau^5 + O(\tau^6), \tag{A9}$$

for $(\bar{2})$. Accordingly, both schemes give as the stability condition, $\tau \geqslant 0$, or

$$\Delta t \geqslant 2 \sin ku/2. \tag{A10}$$

Condition (A10) has been derived for $\Delta t \sim \Delta t_0$. However, a numerical solution of the full dispersion relation, (A3), confirms that all roots remain stable as $\Delta t \to \infty$. Thus, condition (A10) is necessary and sufficient for stability.

ACKNOWLEDGMENTS

This work was supported by the U.S. Department of Energy, under Contract Number DE-FG05-80ET-53088, the National Science Foundation Grant NSF-ATM81-10539, and by the Ministry of Education of Japan under the U.S./Japan Joint Institute for Fusion Theory (JIFT). One of us (D.C.B.) would like to acknowledge the kind hospitality of the JIPP–Nagoya staff during his stay there when much of this work was begun and the visit of Professor T. Kamimura to IFS–Texas during which this work was completed. The authors have also benefited enormously from discussions with H. Berk, J. U. Brackbill, B. I. Cohen, A. B. Langdon, and M. N. Rosenbluth.

REFERENCES

1. J. M. DAWSON, *in* "Methods of Computational Physics" (B. Alder *et al.*, Eds.), Vol. 9, p. 1, Academic Press, New York, 1970; C. K. BIRDSALL, A. B. LANGDON, AND H. OKUDA, *ibid.*, p. 241.

2. K. V. ROBERTS AND D. E. POTTER, *in* "Methods of Computational Physics" (B. Alder *et al.*, Eds.), Vol. 9, p. 339, Academic Press, New York, 1970; J. V. BRACKBILL, *in* "Methods of Computational Physics" (B. Alder *et al.*, Eds.), Vol. 16, p. 1, Academic Press, New York, 1976.
3. A. B. LANGDON, *J. Comp. Phys.* **30** (1979), 202.
4. R. J. MASON, *J. Comp. Phys.* **41** (1981), 233.
5. J. DENAVIT, *J. Comp. Phys.* **42** (1981), 337.
6. A. FRIEDMAN, A. B. LANGDON, AND B. I. COHEN, *Comm. Plasma Phys. Contr. Fusion* **6** (1981), 225.
7. B. I. COHEN, A. B. LANGDON, AND A. FRIEDMAN, *J. Comp. Phys.* **46** (1982), 15.
8. A. B. LANGDON, B. I. COHEN, AND A. FRIEDMAN, *J. Comp. Phys.* **51** (1983), 107.
9. J. U. BRACKBILL AND D. W. FORSLUND, *J. Comp. Phys.* **46** (1982), 271.
10. D. C. BARNES AND T. KAMIMURA, Institute of Plasma Physics, Nagoya University, Research Rept. No. IPPJ-570, 1982; D. C. BARNES AND T. KAMIMURA, *Bull. Amer. Phys. Soc.* **26** (1981), 986.
11. T. TAJIMA AND J. N. LEBOEUF, *Bull. Amer. Phys. Soc.* **26** (1981), 986.
12. T. KAMIMURA, T. TAJIMA, J. N. LEBOEUF, AND D. C. BARNES, *Bull. Amer. Phys. Soc.* **27** (1982), 1035.
13. J. N. LEBOEUF AND T. TAJIMA, *in* "Proceedings of the Annual Sherwood Controlled Fusion Theory Conference," p. 1E9, Santa Fe, New Mexico, April 25–28, 1982.
14. W. L. KRUER, J. M. DAWSON, AND B. ROSEN, *J. Comp. Phys.* **13** (1973), 114.
15. H. OKUDA, A. T. LIN, C. C. LIN, AND J. M. DAWSON, *Comp. Phys. Comm.* **17** (1979), 227.
16. O. BUNEMANN, *J. Comp. Phys.* **1** (1967), 517.
17. J. P. BORIS, *in* "Proceedings, Fourth Conference on Numerical Simulation of Plasma" (Boris and Shanny, Eds.), p. 4, U.S. Govt. Printing Office, Washington D.C. (Stk. No. 0851-0059), 1970.
18. A. Y. AYDEMIR, D. C. BARNES, AND T. KAMIMURA, *in* "Proceedings, Annual Sherwood Controlled Fusion Theory Conference," p. 1E17, Santa Fe, New Mexico, April 25–28, 1982.
19. T. G. NORTHRUP, *Ann. of Phys.* **15** (1961), 19.
20. B. I. COHEN, T. A. BRENGLE, D. B. CONLEY, AND R. P. FRIES, *J. Comp. Phys.* **38** (1980), 45; B. I. COHEN, R. P. FRIES, AND V. THOMAS, *J. Comp. Phys.* **45** (1982), 345.
21. A. B. LANGDON, private communication, 1982.
22. C. W. NIELSEN AND H. R. LEWIS, *in* "Methods of Computational Physics" (B. Alder *et al.*, Eds.), Vol. 16, p. 367, Academic Press, New York, 1976; J. BUSNARDO-NETO, P. L. PRITCHETT, A. T. LIN, AND J. M. DAWSON, *J. Comp. Phys.* **23** (1977), 300.
23. P. CONCUS AND G. H. GOLUB, *SIAM J. Numer. Anal.* **10** (1973), 1103.
24. H. OKUDA, J. M. DAWSON, A. T. LIN, AND C. C. LIN, *Phys. Fluids* **21** (1978), 476.
25. N. A. KRALL AND A. W. TRIVELPIECE, "Principles of Plasma Physics," McGraw–Hill, New York, 1973.
26. A. B. MIKHAILOVSKII, "Theory of Plasma Instabilities," Vol. 2, p. 114, Consultants Bureau, New York/London, 1974.